JOURNAL OF COMPUTATIONAL PHYSICS 110, 103–111 (1994)

Numerical Study of Pseudospectral Methods in Shock Wave Applications

WAI SUN DON

Division of Applied Mathematics, Brown University, Providence, Rhode Island 02912

Received November 28, 1990; revised April 8, 1993

In this paper we use shock capturing spectral methods to simulate compressible flows in the presence of shock waves. Three applications are considered. The first is an interaction of a one-dimensional shock with an entropy wave. The second case deals with interactions between shock wave and an entropy wave in two space dimensions and the third case is two-dimensional shock–vortex interactions. The first two applications are found in the study of turbulence in high speed flow. The last application is a key element in understanding the acoustic dynamics in aeroacoustic and in design of supersonic jet in aerodynamics. The purpose of this study is to show the feasibility of simulating shocked flow with spectral methods. The numerical methods involved are the Chebyshev and Fourier collocation methods. The Euler equations of gas dynamics is discretized by pseudospectral (collocation) methods in space and a nonlinearly stable third-order Runge–Kutta method in time. The fluxes are evaluated pointwise directly and not by the cell-averaging technique. A significant reduction in CPU time and storage usage are achieved by incorporating several well-established numerical techniques, such as grid transformation and filtering, into the spectral algorithm. The results of this study indicate that spectral method is well suited not only for smooth problems but also for those with discontinuity.

1. INTRODUCTION

In the numerical simulation of turbulence, high order methods are essential in capturing the fine scale and delicate physical phenomenon. Spectral methods, with their minimum dispersive and dissipative errors and high order of accuracy, have been applied successfully to such problems in which the solutions are smooth and well behaved at any finite time. However, those methods, owing to their global representation of the data, develop global oscillations due to the Gibbs phenomenon when applied to problems with discontinuities. These oscillations often destroy the accuracy of the spectral methods and cause nonlinear instability. Applications of spectral methods to inviscid compressible flow (Euler equations) are much less developed, due to the shock formation by the nonlinearity of the equations, than incompressible fluid flows.

Previous studies of spectral methods applied to shock wave calculations indicate that the Gibbs phenomenon can be overcome. Gottlieb and Tadmor [9] proved that, for linear problems, the moments of the numerical solution computed by spectral methods are spectrally accurate. Moreover, Lax [16] had argued that more information about the solution is contained in high resolution schemes, even for nonlinear problems. The latest result by Tadmor [27] shows the convergence of the spectral methods for nonlinear scalar equations. Numerous numerical experiments in shock simulation using spectral approximation (see, for example, [2, 3, 5, 28]) had also demonstrated the validity of these theoretical results. Most of those numerical experiments, with the exception of [2], were limited to shocks composed only by piecewise linear functions without any fine structure. In [2], good results were obtained to shock–entropy wave interaction by using the Chebyshev collocation method and a cell-averaging technique for the numerical fluxes, which is a smoother quantity than the pointwise one. Furthermore, spectral accuracy away from discontinuity was demonstrated. However, these results were one-dimensional. The only two-dimensional problem considered in [2] was a scalar one.

In this paper, we apply spectral methods to some practical two-dimensional fluid flow problems with large and fine flow structures along with the shock. For multi-dimensional nonlinear system of partial differential equations, the cell averaging technique developed in [2] is difficult to implement efficiently. Instead, we use the pointwise formulation of Chebyshev and Fourier collocation methods. Several numerical techniques are incorporated in the algorithm to allow a significant reduction of computer resources in terms of CPU time and storage usage. One of those numerical techniques, in particular, worth mentioning is a grid-mapping technique [15] developed by Kosloff and Tal-Ezer. By redistributing the Chebyshev collocation points to an almost uniformly spaced grid, it allows fewer grid points and a larger time step to be taken in this study. The shock is captured very well and small-scale structures are well resolved. We emphasize that in this paper we do not

0021-9991/94 $6.00

use the any fancy nonlinear fixes, e.g., the "essentially non-oscillatory" spectral method developed in [3]. Instead, we keep the spectral scheme stable by a weak exponential filter at every time step. At the final time step, the oscillatory solution is post-processed to recover an almost oscillation-free solution. As shown in [1], oscillatory solution computed by the spectral scheme contains high order information about strength and location of the shock.

Moreover, the author would like to stress that the numerical algorithm presented in this study is an *oscillatory spectral shock-capturing method.* It should not be confused with a *spectral shock-fitting method* in which the shock is fitted as a computational boundary. The advantage of shock fitting is that the underlining solution is smooth, hence great accuracy can be achieved with fewer numbers of basis function. The main disadvantage is that the shock-fitting method is limited for problems with well-defined shock fronts [13, 23].

Other classes of numerical methods most commonly used in the study of shock wave calculation are finite-difference techniques, most notably, the "essentially non-oscillatory" schemes (ENO) [10]. To minimize numerical oscillations, ENO schemes biased the stencil locally in computing derivatives to avoid differencing across the discontinuity. For comparison purposes, solutions computed by the spectral methods are compared with the one computed by the ENO third-order finite-difference scheme [24–26].

This paper is organized as follows. In Section 2 we describe the nuts and bolts of the numerical techniques used in this research. Sections 3.1, 3.2, and 3.3 present the results of the simulations in one-dimensional shock–entropy wave interaction, two-dimensional shock–entropy wave interaction, and two-dimensional shock–vortex interaction, respectively. Concluding remarks are given at the end of the Section 3.3.

2. NUMERICAL METHODS

Consider the 2D Euler equations for gas dynamics in strong conservation form

$$\frac{\partial \mathbf{W}}{\partial t}+\frac{\partial \mathbf{F}}{\partial x}+\frac{\partial \mathbf{G}}{\partial y}=0, \tag{2.1}$$

where the vector of unknown is $\mathbf{W}=[\rho, m, n, E]^{\mathrm{T}}$ and the fluxes are given by

$$\mathbf{F}=\left[m, \frac{m^2}{\rho}+P, \frac{mn}{\rho}, (E+P)\frac{m}{\rho}\right]^{\mathrm{T}},$$

$$\mathbf{G}=\left[n, \frac{mn}{\rho}, \frac{n^2}{\rho}+P, (E+P)\frac{n}{\rho}\right]^{\mathrm{T}},$$

where ρ, m, n, and E are, respectively, the density, mass flux in x, mass flux in y, and total energy per unit volume. It is coupled with the equation of state for ideal gas, $P=(\gamma-1)(E-\frac{1}{2}(m^2+n^2)/\rho)$ and the ratio of specific heats $\gamma=1.4$.

The physical domain has a finite length in x direction and either bounded or unbounded, depending on the physical problem being considered, in the y direction. The physical domain is mapped into a rectangular computational domain (ξ, η), with $-1\leqslant\xi, \eta\leqslant 1$ or $0\leqslant\eta\leqslant 2\pi$ in the case of a periodic boundary in y. The transformation of the infinite domain into finite domain is accomplished by the tangent mapping, i.e., $y=\kappa\tan(\pi\eta/2)$ ($\kappa=0.2$–0.4 typically).

The system (2.1) is discretized in the computational domain (ξ, η) by the Chebyshev collocation (pseudospectral) method in ξ and either Chebyshev or Fourier collocation method in η. These two collocation methods are well documented. The reader is referred to [4, 8, 30] *et al.* for a detailed discussion of these methods. We now discuss in detail some of the non-standard numerical techniques employed in this algorithm:

1. It is well known that the differentiation of a function using Chebyshev and Fourier collocation methods can be evaluated either by fast Fourier transform (FFT) or by matrix–vector multiplication technique. In the matrix–vector multiplication technique used, we applied the even–odd function decomposition idea advocated by A. Solomonoff [22], the computational time can be reduced by as much as 35%. We will briefly describe this new method.

In evaluating the derivative of a given function f by Chebyshev collocation method (for example), the value of f at the grid point ξ_i is factored into $f_i=e_i+o_i$, $i=0, ..., N$, where e and o are the even and odd parts of f, respectively. The entries of the Chebyshev differentiation matrix (see [30]) satisfy the relation $d_{i,j}=-d_{N-i,N-j}$. Assuming N is odd,

$$e_i'=-e_{N-i}'=\sum_{j=0}^{(N-1)/2}(d_{i,j}+d_{i,N-j})\,e_j \tag{2.2}$$

$$o_i'=o_{N-i}'=\sum_{j=0}^{(N-1)/2}(d_{i,j}-d_{i,N-j})\,o_j, \tag{2.3}$$

where the superscript $'$ denotes differentiation. Finally, $f_i'=e_i'+o_i'$ and $f_{N-i}'=-e_i'+o_i'$ for $i=0, ..., (N-1)/2$. With a slight modification, the same idea is also applicable for even N (i.e., odd number of grid points). The total count of operations of this algorithm reduced to $O(N^2/2)$ as compared to $O(N^2)$ for the normal matrix–vector multiplication method. Moreover, the total storage requirement for the even and odd differentiation matrices are $N^2/2$ as oppose to N^2 for the full differentiation matrices. Similar algorithm can be applied to both the Chebyshev and Fourier collocation methods.

2. A third-order TVD (total variation diminishing) Runge–Kutta method [24] is used to march the Euler equations in time. It has the form of

$$\mathbf{W}^1 = \mathbf{W}^n - \Delta t\, L(\mathbf{W}^n)$$
$$\mathbf{W}^2 = \tfrac{1}{4}(3\mathbf{W}^n + \mathbf{W}^1 - \Delta t\, L(\mathbf{W}^1)$$
$$\mathbf{W}^{n+1} = \tfrac{1}{3}(\mathbf{W}^n + 2\mathbf{W}^2 - 2\,\Delta t\, L(\mathbf{W}^2),$$

where L is the spatial operator for the fluxes. Under suitable $CFL \leqslant 1$, this method is TVD-stable if the Euler forward version of the spatial operator L is TVD. It should be noted, however, that L is not TVD under our formulation.

It is well known that, for the Chebyshev collocation method, the CFL condition for stability restricts the time step $\Delta t \leqslant \text{Const} \cdot N^2$, where N is the number of collocation points taken [9]. To alleviate the severe restriction imposed on the time step Δt, we transformed the Chebyshev collocation points $\{\xi_j = \cos(\pi j/N),\ j = 0, ..., N\}$ by the mapping [15],

$$\bar{x}(\xi) = \frac{\sin^{-1}(\beta\xi)}{\sin^{-1}(\beta)}. \tag{2.4}$$

By taking $\beta = 0.999$, the new grid points $\bar{x}(\xi_j)$'s are almost evenly spaced! This transformation serves two important purposes. First, larger (approx. 10 times) CFL numbers can be used while maintaining stability of the spectral scheme. One can imagine that the Const in the CFL condition is multiplied by a large coefficient, namely the metric tensor of the mapping. Second, the resolution around the center of the physical domain, where most of the relevant physical phenomenon is located, improves dramatically. Hence, fewer collocation points are needed, which in turn further relaxes the CFL condition. Without this mapping technique, serious difficulties will be encountered in terms of computing resources for a fixed resolution requirement. By the way, one can take CFL as big as three, in practice, for this algorithm.

3. Despite the fact that the CFL condition on Δt is strictly enforced, oscillations generated by the Gibbs phenomenon grow in time and the scheme becomes unstable eventually. In order to control the nonlinear growth of oscillation, and exponential filter [30]

$$\sigma_k = e^{-\alpha(k/N)^\gamma}, \qquad 0 \leqslant |k| \leqslant N, \tag{2.5}$$

is used to modify the Fourier and/or Chebyshev coefficient of index k. More precisely, suppose the function $f(x)$ allows an expansion in terms of a Chebyshev polynomial of degree N,

$$f(x) = \sum_{k=0}^{N} a_k T_k(x).$$

The filtered function $\hat{f}$ becomes

$$\hat{f}(x) = \sum_{k=0}^{N} \sigma_k a_k T_k(x).$$

This procedure can be implemented efficiently either by the fast Fourier algorithm or by the matrix vector multiplication technique.

Our experience indicated that the filter should be applied to the derivatives of the fluxes $\mathbf{F}$, $\mathbf{G}$, and solution $\mathbf{W}$ at every time step. However, it is not necessary to apply filtering of $\mathbf{W}$ at the first and second stages of the TVD Runge–Kutta scheme. In most cases, a weak filter of order $\gamma = 16$ and $\alpha = 32.23619$ is sufficient. For strong shock interaction with strong structures, for example, vortex with strong circulation, a filter of order 12, along with larger N, should be used. In practice, once the instability subsided, one can revert to a weaker filter to continue the simulation. The general guideline regarding the order of filter is that one should use a little filtering as possible but just strong enough to stabilize the calculation.

Theoretically, the exponential filter recovers solution with spectral accuracy away from the discontinuity only for the Fourier method. Numerically, the same result seems to hold true also for the Chebyshev method. The optimal filter, developed by Vandeven [29], which linked the order of filtering to the number of collocation points (or modes), offers an attractive alternative for the exponential filter used here. Other filtering functions, such as sharpened raised cosine etc., can also be considered for the substitution of the exponential filter. Research in the effect of filtering on the accuracy of the Chebyshev method is an important subject and will be studied in the future.

4. It is well known that great care should be exercised in the application of boundary conditions when spectral methods are used to solve the hyperbolic system of equations. The characteristic treatment based on the eigenvalues of the linearized one-dimensional Euler equations of gas dynamics is used at each boundary points in the x direction. Readers are referred to [6] for details. If the domain in y is unbounded, the boundary points are assigned values as computed by the spectral scheme. Naturally, periodic boundary conditions are applied if the problem being study is periodic in y as in Example 2 of next section.

5. Once the final time has been reached, the computed oscillatory solution will be processed through the reconstruction step in order to recover a non-oscillatory solution. The underlying theory behind this procedure is simply that, for linear problems, the moments of the numerical solution computed by spectral methods are spectrally accurate [9]. Moreover, Lax [16] had argued that more information about the solution is contained in high resolution schemes, even for nonlinear problems. Under this

framework, the problem of constructing a non-oscillatory solution from the noisy solution becomes the problem of signal processing. That is, how to reconstruct a meaningful result from the noisy data? Several techniques had been developed with some success for both the Fourier and Chebyshev methods [1, 3, 5]. The procedure used in this research consisted of two steps (see [1] for details).

1. The location x_s and the strength A of the discontinuity are determined from the moments of the oscillatory solution $f_N(x)$ by a least square fit of $f_N(x)$ and a step function $S_N(x)$.

2. $\hat{f}_N(x) = \mathcal{F}(f_N(x) - S_N(x)) + S(x)$,

where $\mathcal{F}$ is the filtering (smoothing) operator, S is the Heaviside function with jump A at x_s, and S_N is the N-degree polynomial approximation of S.

This particular procedure is, by no means, optimal. Research for a better reconstruction step is currently under intensive investigation. In the y direction, the solution is simply smoothed by the exponential filter ($\gamma = 3$, typically). No attempt had been made to reconstruct the solution in y.

6. Furthermore, with a simple change of the variables $x' = x - v_s t$, $t' = t$, we can switch the frame of reference to the shock. In other words, the shock is almost fixed around some given location in the physical domain while the upstream disturbance is being passed through the shock. All disturbances including the vortex can be introduced into the flow field by modified boundary conditions. Within this framework, it is possible to have a fixed finite physical domain in x and an arbitrarily large terminal time. This technique had been applied successfully to problems discussed in next section along with the normal moving shock cases. It is particularly beneficial if physical phenomenon is sought for large final time with a fixed resolution requirement.

In this study we shall refer to this numerical scheme as the *spectral scheme*.

3. NUMERICAL EXPERIMENTS

All the computations are performed on the Cray 2 supercomputer at Phillips Laboratory Supercomputer Center of Kirtland Airforce Base. Depending on the problem size, either the FFT or matrix–vector multiplication technique is used to compute derivatives of flux. In contrast to the ENO technique, there is no decision making step required to determine the smoothness of the derivatives by biasing the stencils, at each grid point. This allows a thorough vectorization in those computationally intensive routines, mainly, the Runge–Kutta step and the differentiation routines. Furthermore, with the matrix–vector multiplication and the even–odd decomposition techniques mentioned earlier, CPU time usage can be reduced by as much as 35%.

3.1. *One-Dimensional Shock–Entropy Wave Interaction*

The first numerical problem we tested our algorithm is a Mach 3 shock interacting with a entropy sine wave, i.e., initially,

$$(\rho, u, P) = \begin{cases} (3.857143,\ 2.629369,\ 10.33333) \\ \quad \text{if} \quad x < -0.8 \\ (1 + \varepsilon \sin(k\pi x),\ 0,\ 1) \\ \quad \text{if} \quad x > -0.8, \end{cases} \tag{3.1}$$

where $\varepsilon = 0.2$ and $k = 5$.

This problem had been used extensively in testing the capability of many different numerical schemes, e.g., the second-order MUSCL scheme [19], ENO [25], spectral shock fitting [12]. It is because the result of the interaction of the shock with a small-amplitude low-frequency density disturbance generates a large-amplitude high-frequency entropy wave behind the shock. Low order schemes, in general, had not been able to capture this fine structure. Figures 1, 2; 3, 4; 5, 6 showed the solution of density before and after reconstruction with three different grid sizes $N = 160, 256, 512$, respectively, at time $T = 1.80$. The solid line is the solution computed by the third-order ENO with 1200 points that we take as a converged solution.

In summary, despite the Gibbs phenomenon and nonlinearity of the Euler equations, the complicated flow field is well resolved and the main shock remains sharp within one grid cell, even with this naive approach of using spectral methods. As evident in the solution, an additional small shock is formed behind the main shock. The Gibbs phenomenon is quite obvious since we do not attempt to locate this shock intentionally. Until a reliable algorithm for

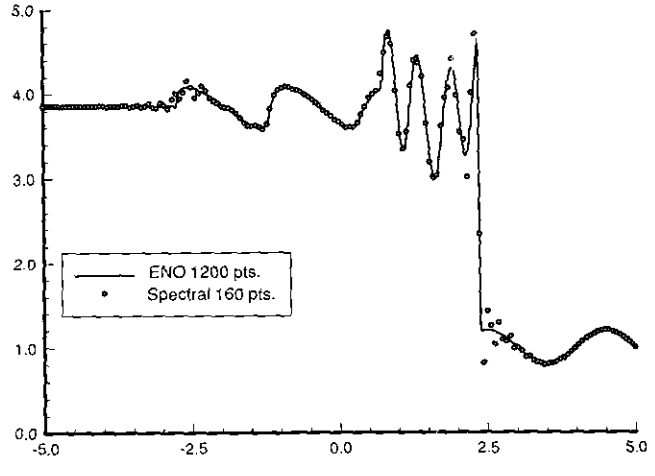

FIG. 1. 1D shock–entropy wave interaction, $N = 160$, pre-processed density solution.

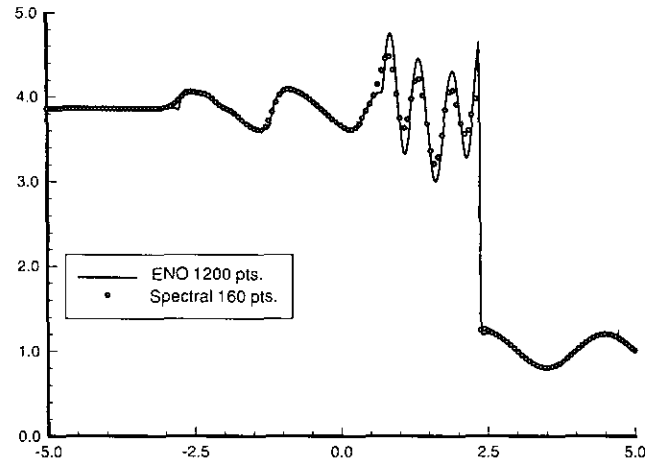

FIG. 2. 1D shock–entropy wave interaction, $N = 160$, post-processed density solution.

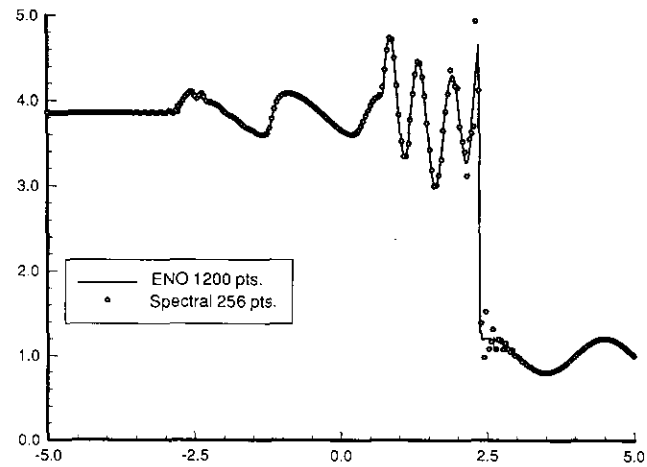

FIG. 3. 1D shock–entropy wave interaction, $N = 256$, pre-processed density solution.

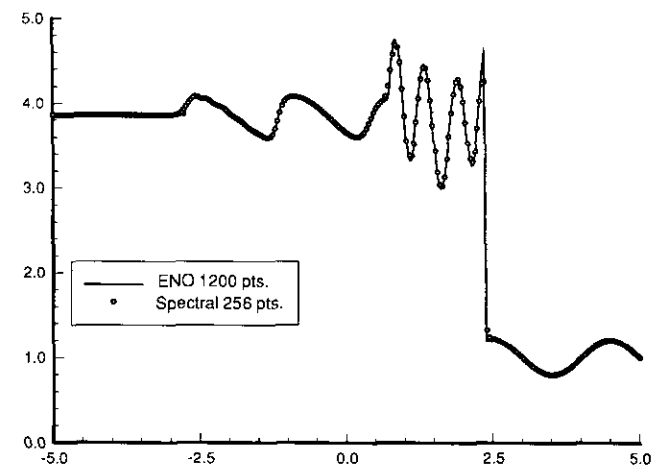

FIG. 4. 1D shock–entropy wave interaction, $N = 256$, post-processed density solution.

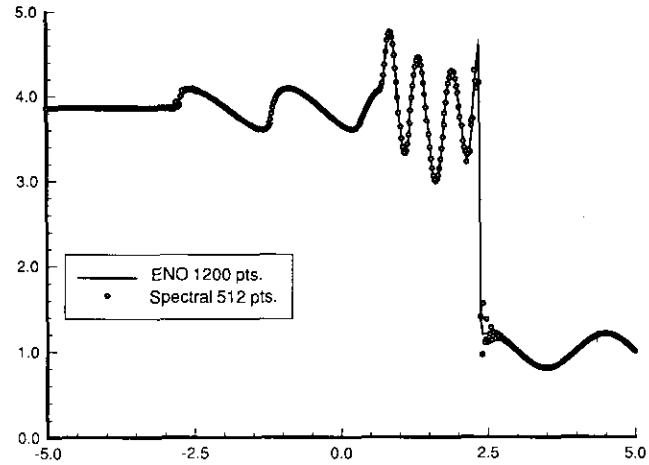

FIG. 5. 1D shock–entropy wave interaction, $N = 512$, pre-processed density solution.

locating multiple shocks is found, we will leave the solution as computed with this algorithm.

3.2. *Two-Dimensional Shock–Entropy Wave Interaction*

We also used our spectral code to study the linear amplification factors of a small entropy disturbance, interacting with a shock wave, as a function of the angle between the shock and the disturbance. This problem arises from the study of two-dimensional homogeneous compressible turbulence with shocks. Readers are referred to [31] for detailed discussion of the modeling and analysis of this problem. Spectral methods, by nature of their high accuracy and negligible dispersive and dissipative errors, are ideally suited to the numerical study of shock-free turbulence. Here we would like to argue the applicability of the spectral methods to the shock–turbulence interactions. In order to investigate this issue, the small eddy turbulence is modeled

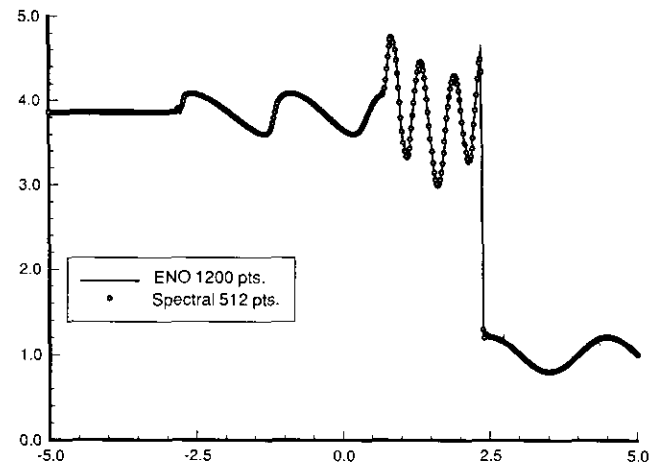

FIG. 6. 1D shock–entropy wave interaction, $N = 512$, post-processed density solution.

by a small entropy wave in various angles relative to the shock front. In this case, analytical linear analysis of the entropy amplification factors provided a needed reference for the accuracy of this simulation.

The initial conditions are defined as follows: The right state of the shock is given as $(\rho_r, u_r, v_r, P_r) = (1, 0, 0, 1)$. With a given shock Mach number M_s, the flow conditions across the shock are evaluated via the Rankine–Hugoniot jump conditions, i.e.,

$$\begin{aligned} P_l &= P_r\left(\frac{2\gamma\bar{M}^2-(\gamma-1)}{(\gamma+1)}\right) \\ \rho_l &= \rho_r\left(\frac{(\gamma+1)\bar{M}^2}{(\gamma-1)\bar{M}^2+2}\right) \\ u_l &= v_s+(u_r-v_s)\,\rho_r/\rho_l \\ v_l &= 0, \end{aligned} \tag{3.2}$$

where

$$c_r=\sqrt{\gamma(P_r/\rho_r)}, \qquad v_s=M_s c_r, \qquad \bar{M}=\frac{u_r-v_s}{c_r}.$$

The solution of (3.2) is a pure shock moving to the right with shock speed v_s. For our problem the density ρ_r in the right state of the shock is multiplied by ρ_ε,

$$\rho_\varepsilon = e^{-(\varepsilon/P_r)\cos(k\pi(x\cos\theta + y\sin\theta))}, \tag{3.3}$$

where ε, k, and θ are the amplitude, wave number, and angle, relative to the normal shock, of the entropy perturbation wave. The physical domain is $-5 \leqslant x \leqslant 5$ and $0 \leqslant y \leqslant 2/(k \sin\theta)$. Since the entropy wave is assumed to be periodic in y, the Chebyshev and Fourier collocation methods are used in the x and y directions, respectively.

In this simulation, the shock compresses the entropy wave upstream into waves with higher wave number downstream behind the shock. To analyze the process one has to carry out a very long time integration. In most cases, the shock would have moved beyond the physical domain. There are two ways to remedy this situation. One way is to enlarge the physical domain in such a way that the shock remains inside the domain at the terminal time at the expense of resolution for a given number of collocation points. The second way is to use the change of variables technique mentioned in last section to keep the shock in the domain while the entropy wave is introduced through the boundary conditions. Obviously, for the reasons stated previously, the latter method is preferred in this simulation.

Table I gives the relative error (in percentage) of the computed linear amplification factors of the entropy wave in comparison with the analytical one given by linear theory.

TABLE I

Relative Error of the Shock–Entropy Wave Interaction

M_s	θ	ε	k	N_x, N_y	Relative error (percentage)
2	30	0.02	2	192, 32	3.5
3	10	0.02	2	192, 32	3.9
3	30	0.02	2	192, 32	4.4
3	50	0.02	2	192, 32	5.3
5	30	0.02	2	256, 48	4.6
8	10	0.02	1	384, 24	3.7
8	30	0.02	1	384, 24	4.1
8	50	0.02	1	384, 24	5.1

The computed amplification factors are computed by averaging the data in some region behind the discontinuity. Hence the relative error shown here might vary depending on the region where the data are used for averaging. The results show a good agreement with parameters ranging from a weak shock ($M_s = 2$) to a strong shock ($M_s = 8$), along with three different entropy waves angles $\theta = 10°, 30°, 50°$. The typical relative error computed by ENO ranges between 4% and 5% [26].

3.3. *Two-Dimensional Shock–Vortex Interaction*

Finally, we computed the solution of the shock–vortex interactions. A better understanding of the physics of the shock–vortex interactions has many potential applications, e.g., supersonic and subsonic jet nozzle design. Because of the high non-linearity of the interaction, its physics is not well understood, in general, with the exception of the linear analysis done by Ribner and Moore [21, 18]. According to their linear analysis, an acoustic radiation pattern (sound wave) will be generated by interaction. As stated in [17], the sound wave will have a significant impact on the design of jet engines that operate at supercritical nozzle pressure ratios and helicopter blades designed for operating at supercritical speeds. This problem had been investigated by many researchers using various numerical techniques. The second-order MacCormack finite difference method [20], the upwind finite volume method [17], and spectral shock fitting methods [11, 13, 14, 23] were used with various degrees of success and limitation. In most of their research in this application, the shock Mach number and vortex strength used was relatively weak, compared with some of the cases studied here. Moreover, most of the earlier works done in this area using spectral methods are shock fitting techniques. They gave better accuracy but cannot handle a complicated solution like shock bifurcation. (*Note.* The recent paper "Uniform High Order Spectral Methods for One and Two Dimensional Euler Equations" by Cai and Shu had simulated this problem successfully, see ICASE Report 91-26 for the details.)

Following the definition of a vortex used in [13], the tangential velocity profile of the vortex centered at $(x_c, y_c) = (1.1, 0)$ in polar coordinates is

$$U(r) = \begin{cases} \Gamma r(r_0^{-2} - r_1^{-2}), & 0 \leqslant r \leqslant r_0 < r_1, \\ \Gamma r(r^{-2} - r_1^{-2}), & r_0 \leqslant r \leqslant r_1, \\ 0, & r > r_1, \end{cases} \tag{3.4}$$

where $r_0 = 0.2$ and $r_1 = 1.0$ unless specified otherwise. The Chebyshev collocation method is used in both the x and the y directions. This vortex is rotating in a counterclockwise direction. Hence, the velocity field upstream of the shock becomes

$$\begin{aligned} u &= u_r - U(r) \sin\theta \\ v &= v_r + U(r) \cos\theta, \end{aligned} \tag{3.5}$$

where $\theta = \tan^{-1}((y - y_c)/(x - x_c))$.

In order to test this algorithm to its full potential, we have simulated this problem with various shock Mach numbers M_s and vortex strengths Γ.

Figure 7 shows the pressure contour plot for shock Mach number $M_s = 1.25$, $\Gamma = 0.02$. The physical domain is $0 \leqslant x \leqslant 3$ and $-2 \leqslant y \leqslant 2$. The Tal-Ezer mapping is used in both directions with $\beta = 0.999$. The grid size used is 128^2. The shock is located at $x = 0.5$ initially. Both the flux derivatives and solution are filtered with a $\gamma = 16$-order exponential filter. The oscillatory solution is post-processed with $\gamma = 3$ at final time $T = 1.25$. This computation consumed a total CPU time of 112 s for 412 time steps.

By drawing an imaginary circular arc from the center of the vortex, one can clearly see that an acoustic wavefront is generated by the shock–vortex interaction. One should note that the parameters used here is the same one used in [13], except that the final termination time is not available in the reference. In contrast to the single domain Chebyshev collocation result shown in [13], the flow field is well resolved and qualitatively similar to the multidomain calculation after post-processing.

In [17], similar problems were simulated by a second-order upwind finite volume method with flux vector splitting. Deformation and bifurcation of the shock were observed when the vortex strength is "strong" relative to the shock strength. Since different definitions of the vortex are used in [17] and this study, no direct comparison will be made in this case.

However, we observed a similar deformation and bifurcation of the shock for the case of $M_s = 3$ and $\Gamma = 0.25$ (as well as in some other cases) as shown in the pressure contour plot later. For this case, we used the $\gamma = 16$-order filtering on the flux derivatives and $\gamma = 14$ for the solution. The final solution is post-processed with $\gamma = 3$ at the final time $T = 0.5$. All other parameters are the same as the $M_s = 1.25$ case. The total CPU time used is 115 (556) s with 410 (520) time steps for the grid 128^2 (256^2).

Before the reconstruction step, the raw pressure contour data of grid size 128^2 are plotted in Fig. 8. One can see that the solution is highly oscillatory and that the fine scale features are badly contaminated by the numerical noise. After post-processing, the numerical noise is removed from the data by the reconstruction procedure. The pressure contour plot (Fig. 9) shows a greatly improved solution almost free of oscillation away from the shock front. Small scale and deep gradient are recovered with good accuracy. Figure 10 shows the pressure contour plot for grid size of 256^2. The fine grid solution agrees very well with the coarse one.

To verify the spectral result, we compare the results with the one computed by the ENO third-order scheme using the same parameters, except the grid size is 128 in x and 64 in y. Figure 11 shows the pressure contour plot of ENO third-order scheme [Shu, private communication]. In Fig. 12, the

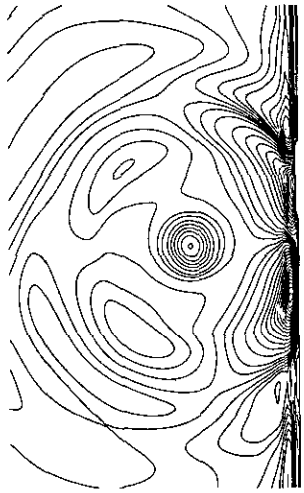

FIG. 7. 2D shock–vortex interaction, $M_s = 1.25$, $\Gamma = 0.02$.

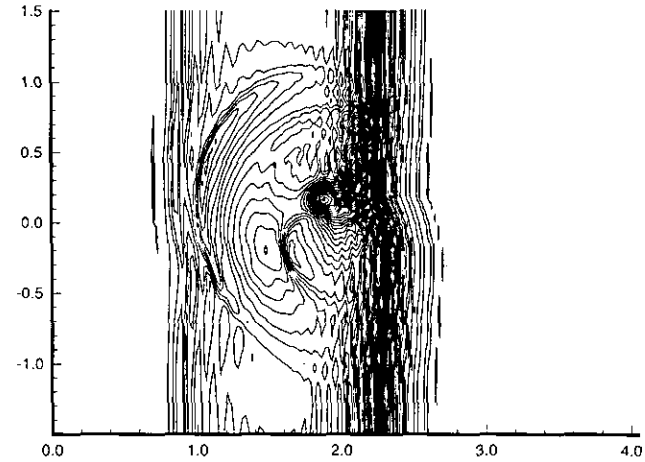

FIG. 8. 2D shock–vortex interaction, pressure contour, raw data, $M_s = 3.0$, $\Gamma = 0.25$, $N_x = 128$, $N_y = 128$.

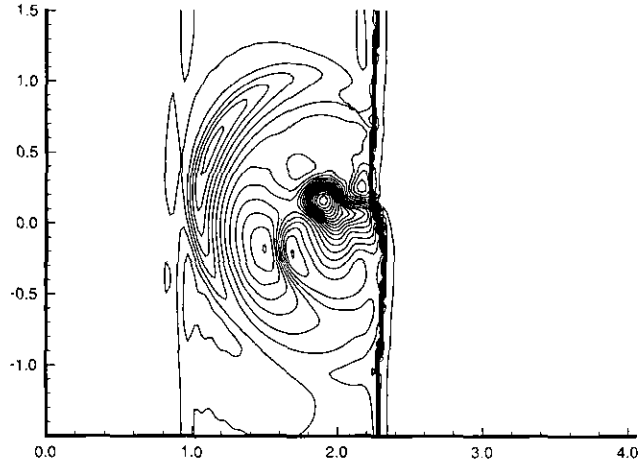

FIG. 9. 2D shock–vortex interaction, pressure contour, $M_s = 3.0$, $\Gamma = 0.25$, $N_x = 128$, $N_y = 128$.

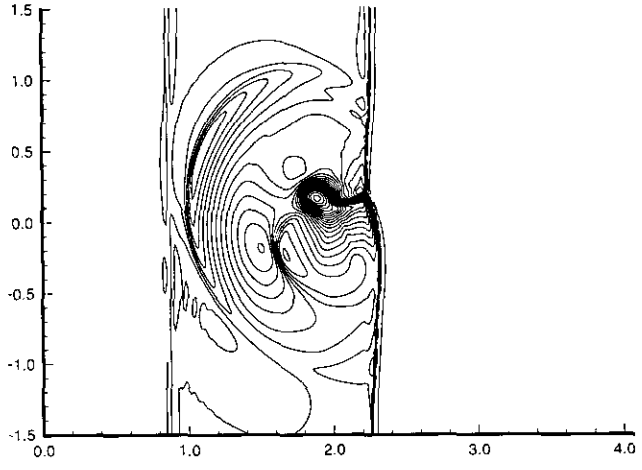

FIG. 10. 2D shock–vortex interaction, pressure contour, $M_s = 3.0$, $\Gamma = 0.25$, $N_x = 256$, $N_y = 256$.

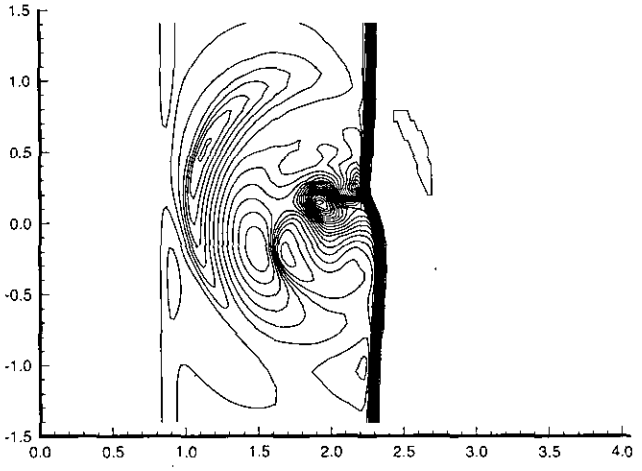

FIG. 11. 2D shock–vortex interaction, pressure contour, $M_s = 3.0$, $\Gamma = 0.25$, $N_x = 128$, $N_y = 64$, computed by ENO third-order scheme.

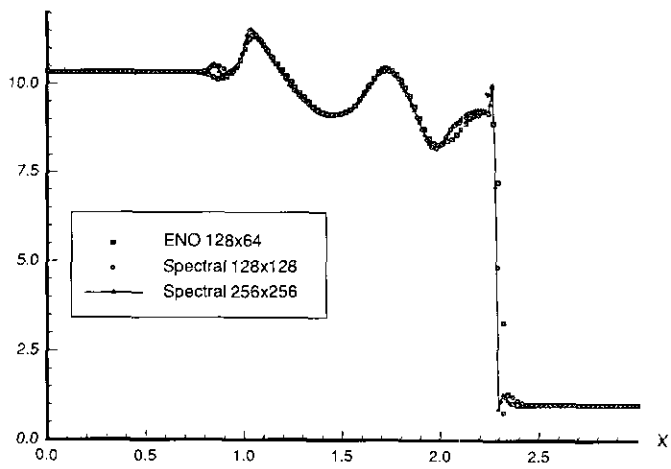

FIG. 12. 2D shock–vortex interaction, pressure contours plotted together, $M_s = 3.0$, $\Gamma = 0.25$. Pressure distribution at $y = 0$ for ENO and spectral schemes.

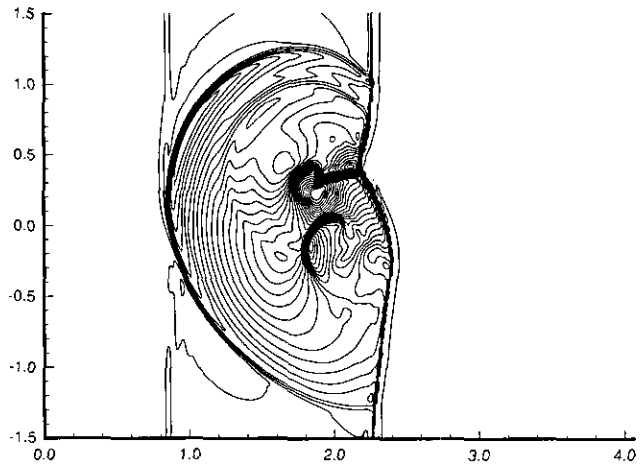

FIG. 13. 2D shock–vortex interaction, pressure contour, $M_s = 3.0$, $\Gamma = 0.5$, $N_x = 256$, $N_y = 96$.

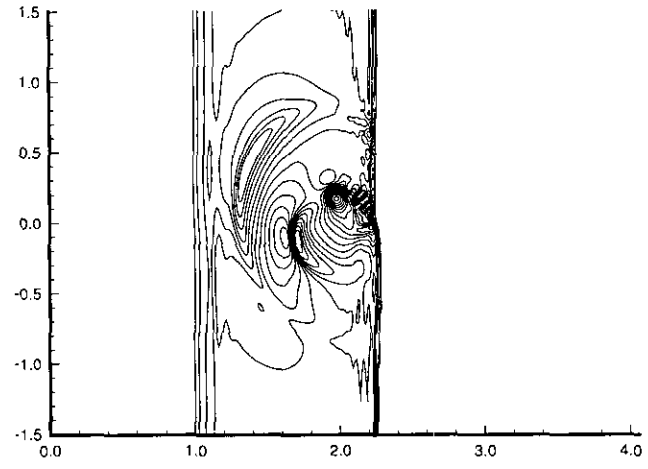

FIG. 14. 2D shock–vortex interaction pressure contour, $M_s = 6.0$, $\Gamma = 0.25$, $N_x = 256$, $N_y = 96$.

pressure data at $y=0$ is taken from these three cases and plotted together. Except for the differences at the end of the wavefront and the shock front, the spectral results agree well with the ENO result.

The applicability of spectral shock calculation is not limited to low shock Mach number and low vortex strength, high Mach number flow up to Mach 6 and vortex strength up to 0.5 have been simulated successfully. The pressure contour plot for cases of ($M_s=3$, $\Gamma=0.5$) and ($M_s=6$, $\Gamma=0.25$) are shown in Figs. 13 and 14, respectively.

The strong vortex strength (shock) case requires $\gamma=12(8)$ and $\gamma=10(8)$ order of filtering on the flux derivatives and solution respectively on a grid size of 256^2. The final terminal time is $T=0.5(0.25)$. The total CPU time used is 556 (567) s with 520 (510) time steps. All other parameters are the same as for the case of $M_s=3$, $\Gamma=0.25$.

Since the main goal of this research is to study the feasibility and efficiency of spectral shock capturing methods in shock wave simulation with realistic physical applications, the physical implications of the shock–vortex interaction will not be discussed in this paper.

In conclusion, we have presented some encouraging results of shock wave simulations using spectral methods. Despite the results this research presented, many other difficult numerical issues remain and it warrants further detailed investigation, for example, a shock locator method that not only identifies the shock location and strength but that also predicts correctly the number of shocks that exist in a complicated flow solution.

ACKNOWLEDGMENTS

The author thanks Professor David Gottlieb and Professor Chi-Wang Shu for many helpful suggestions and discussion. Research was supported in part by the Air Force Office of Scientific Research Grant AFOSR-93-0090 and by NSF Grant DMS-92-11820.

REFERENCES

1. S. Abarbanel and D. Gottlieb, "Information Content in Spectral Calculations," Progress and Supercomputing in Computational Fluid Dynamics, *Proceedings, U.S.–Israel Workshop, 1985*, edited by E. Murman *et al.*, p. 345.
2. W. Cai, D. Gottlieb, and A. Harten, *Comput. Math. Appl.* **24** (5/6), 37 (1992).
3. W. Cai, D. Gottlieb, and C. W. Shu, *Math. Comput.* **52** (186), 389 (1989).
4. C. Canuto, M. Y. Hussaini, A. Quarteroni, and T. A. Zang, *Spectral Methods in Fluid Dynamics* (Springer-Verlag, New York/Berlin, 1987).
5. D. Gottlieb, L. Lustman, and S. A. Orszag, *SIAM J. Sci. Stat. Comput.* **2**, 296 (1981).
6. W. S. Don and D. Gottlieb, "Spectral Simulation of Unsteady Compressible Flow Past a Circular Cylinder," *Proceedings, ICOSAHOM 89* (Elsevier Science, North Holland, 1989).
7. D. Gottlieb, L. Lustman, and C. S. Streett, "Spectral Methods for Two Dimensional Shocks," in *Spectral Methods for Partial Differential Equations*, edited by R. G. Voigt, D. Gottlieb, and M. Y. Hussaini (SIAM–CBMS, Philadelphia, 1984), p. 79.
8. D. Gottlieb and S. A. Orszag, *Numerical Analysis of Spectral Methods: Theory and Applications*, CBMS Conference Series in Applied Mathematics, Vol. 26 (SIAM, Philadelphia, 1977).
9. D. Gottlieb and E. Tadmor, "Recovering Pointwise Values of Discontinuous Data within Spectral Accuracy," Progress and Supercomputing in Computational Fluid Dynamics, *Proceedings, U.S.–Israel Workshop, 1985*, edited by E. Murman *et al.*, p. 357.
10. A. Harten, *J. Comput. Phys.* **49**, 357 (1983).
11. M. Y. Hussaini, D. A. Kopriva, M. D. Salas, and T. A. Zang, *AIAA J.* **23**, 234 (1985).
12. D. Kopriva, private communication.
13. D. Kopriva, "A Multidomain Spectral Collocation Computation of the Sound Generated by a Shock-Vortex Interaction," in *Computational Acoustics: Algorithms and applications*, Vol. 2, edited by D. Lee and M. H. Schultz (Elsevier Science, North Holland, 1988).
14. D. Kopriva, T. Zang, M. Salas, and M. Hussaini, "Pseudospectral Solution of Two-Dimensional Gas Dynamic Problems," in *Proceedings, 5th GAMM-Conf. on Numerical Methods in Fluid Mechanics*, edited by M. Pandolfi and R. Piva (Vieweg, Braunschweig, 1983), p. 185.
15. D. Kosloff and H. Tal-Ezer, *ICASE Report* 89-71 (unpublished).
16. P. Lax, "Accuracy and Resolution in the Computation of Solutions of Linear and Nonlinear Equations," in *Recent Advances in Numerical Analysis, Proc. Symp., Math. Research Center, University of Wisconsin, 1978* (Academic Press, New York, 1978), p. 107.
17. K. Meadows, A. Kumar, and M. Hussaini, *AIAA Pap.* 89-104 (1989).
18. F. Moore, NACA Report 1165, 1954 (unpublished).
19. S. Osher, *SIAM J. Numer. Anal.* **22**, 947 (1985).
20. S. Pao and M. Salas, *AIAA Pap.* 81-1205 (1981).
21. H. Ribner, NACA Report 1233, 1955 (unpublished).
22. A. Solomonoff, *J. Comput. Phys.* **98** (1), 174 (1992).
23. M. Salas, T. Zang, and M. Hussaini, "Shock Fitted Euler Solutions to Shock-Vortex Interactions," in *Proceedings, 8th International Conference on Numerical Methods in Fluid Dynamics*, edited by E. Drause (Springer-Verlag, New York, 1982), p. 461.
24. C. W. Shu and S. Osher, *J. Comput. Phys.* **77**, 439 (1988).
25. C. W. Shu and S. Osher, *J. Comput. Phys.* **83** (1), 32 (1989).
26. C. W. Shu, T. Zang, G. Erlebacher, D. Whitaker, and S. Osher, *Appl. Numer. Math.* **9**, 45 (1992).
27. E. Tadmor, *SINUM* **26**, 30 (1989).
28. E. Tadmor, "Shock Capturing by the Spectral Viscosity Method," in *Proceedings, ICOSAHOM, '89* (Elsevier Science, North Holland, 1989).
29. H. Vandeven, *J. Sci. Comput.* **24**, 37 (1992).
30. R. G. Voigt, D. Gottlieb, and M. Y. Hussaini (Eds.), *Spectral Methods for Partial Differential Equations* (SIAM–CBMS, Philadelphia, 1984).
31. T. A. Zang, M. Y. Hussaini, and D. M. Bushnell, *AIAA J.* **22**, 13 (1984).